AFRL-RX-WP-TP-2012-0398

GROWTH STRESS IN Si02 FORMED BY OXIDATION OF SiC (PREPRINT)

Randall S. Hay
Composites Branch
Structural Materials Division

JULY 2012
Interim

AIR FORCE RESEARCH LABORATORY
MATERIALS AND MANUFACTURING DIRECTORATE
WRIGHT-PATTERSON AIR FORCE BASE, OH 45433-7750
AIR FORCE MATERIEL COMMAND
UNITED STATES AIR FORCE

REPORT DOCUMENTATION PAGE

Form Approved
OMB No. 0704-0188

1. REPORT DATE *(DD-MM-YY)*	2. REPORT TYPE	3. DATES COVERED *(From - To)*
July 2012	Technical Paper	1 June 2012 – 1 July 2012

4. TITLE AND SUBTITLE
GROWTH STRESS IN Si02 FORMED BY OXIDATION OF SiC (PREPRINT)

5a. CONTRACT NUMBER
In-house

5b. GRANT NUMBER

5c. PROGRAM ELEMENT NUMBER
62102F

6. AUTHOR(S)
Randall S. Hay

5d. PROJECT NUMBER
4347

5e. TASK NUMBER
50

5f. WORK UNIT NUMBER
X06L

7. PERFORMING ORGANIZATION NAME(S) AND ADDRESS(ES)
Composites Branch (AFRL/RXCC)
Structural Materials Division
Air Force Research Laboratory, Materials and Manufacturing Directorate
Wright-Patterson Air Force Base, OH 45433-7750
Air Force Materiel Command, United States Air Force

8. PERFORMING ORGANIZATION REPORT NUMBER
AFRL-RX-WP-TP-2012-0398

9. SPONSORING/MONITORING AGENCY NAME(S) AND ADDRESS(ES)
Air Force Research Laboratory
Materials and Manufacturing Directorate
Wright-Patterson Air Force Base, OH 45433-7750
Air Force Materiel Command
United States Air Force

10. SPONSORING/MONITORING AGENCY ACRONYM(S)
AFRL/RXCC

11. SPONSORING/MONITORING AGENCY REPORT NUMBER(S)
AFRL-RX-WP-TP-2012-0398

12. DISTRIBUTION/AVAILABILITY STATEMENT
Approved for public release; distribution unlimited. Preprint to be submitted to MRS Symposium Proceedings.

13. SUPPLEMENTARY NOTES
This is a work of the U.S. Government and is not subject to copyright protection in the United States. PA Case Number and clearance date: 88ABW-2012-1961, 4 April 2012. This document contains color.

14. ABSTRACT
Growth stresses in amorphous SiO2 scales formed during SiC fiber oxidation were calculated. A numerical method using Deal-Grove oxidation kinetics and shear-stress dependent SiO2 viscosity was used. Initial compressive stresses in SiO2 of ~25 GPa from the 2.2× oxidation volume expansion rapidly relaxes. At >1200°, viscous flow of amorphous SiO2 further relaxes stress to negligible levels. At 700° - 900°C, axial and hoop stress at the GPa level persist in SiO2 near the SiC-SiO2 interface. Radial expansion of the scale causes hoop stress to become tensile, and axial stresses are driven to tensile values by the Poisson effect. These tensile stresses can be >1 GPa for thick scales formed at lower temperatures on surfaces with high curvature. Approximate analytical expressions for growth stress are discussed. Effects of viscosity variation as well as other assumptions and limitations of the calculation method are discussed.

15. SUBJECT TERMS
SiC, Oxidation, Fibers

16. SECURITY CLASSIFICATION OF:			17. LIMITATION OF ABSTRACT:	NUMBER OF PAGES	19a. NAME OF RESPONSIBLE PERSON (Monitor)
a. REPORT	b. ABSTRACT	c. THIS PAGE			Randall S. Hay
Unclassified	Unclassified	Unclassified	SAR	8	19b. TELEPHONE NUMBER *(Include Area Code)* N/A

Growth Stress in SiO_2 Formed by Oxidation of SiC

Randall S. Hay
Air Force Research Laboratory, Materials and Manufacturing Directorate
2230 10th St, Bldg 655, WPAFB, OH

ABSTRACT

Growth stresses in amorphous SiO_2 scales formed during SiC fiber oxidation were calculated. A numerical method using Deal-Grove oxidation kinetics and shear-stress dependent SiO_2 viscosity was used. Initial compressive stresses in SiO_2 of ~25 GPa from the 2.2× oxidation volume expansion rapidly relaxes. At >1200°, viscous flow of amorphous SiO_2 further relaxes stress to negligible levels. At 700° - 900°C, axial and hoop stress at the GPa level persist in SiO_2 near the SiC-SiO_2 interface. Radial expansion of the scale causes hoop stress to become tensile, and axial stresses are driven to tensile values by the Poisson effect. These tensile stresses can be >1 GPa for thick scales formed at lower temperatures on surfaces with high curvature. Approximate analytical expressions for growth stress are discussed. Effects of viscosity variation as well as other assumptions and limitations of the calculation method are discussed.

INTRODUCTION

Constraint of the 2.2× volume expansion during oxidation of SiC to SiO_2 generates very large growth stresses. Microstructural evidence for these stresses exists for crystalline scales. High dislocation densities in crystalline SiO_2 near the SiC-SiO_2 interface are diagnostic of high shear stresses during growth of new scale.[1-2] Axial cracks form in the outer scale from tensile hoop growth stress.[1, 3] Tensile growth stresses may decrease fiber strengths, which is significant for structural applications.

Growth stress has been extensively modeled for silicon oxidation, which has volume expansion similar to SiC oxidation.[4-5] Recent models recognize that flow at high stress is viscoelastic and use the Eyring model for shear-stress dependent viscosity.[6-8] Radial compressive and tensile hoop growth stresses are predicted for oxidation of silicon fibers.[9-10] Axial stresses are generally ignored.[6, 9, 11] For structural fibers this is an important omission, because axial residual stress affects fiber strength. Tensile stress increases silicon oxidation rates,[12-13] and recently this has also been demonstrated for SiC.[14]

A method to calculate all the growth stress components anywhere in a SiO_2 scale formed by oxidation of SiC fibers is presented. The method involves scale discretization and separate calculation for each increment. Calculations are done at temperatures from 700° to 1300°C for amorphous scales. Growth stresses for SiC fibers with different radii are examined. Assumptions and limitations of the method are discussed. Complementary results and a more thorough description of the background information and method are given elsewhere.[15]

METHOD

A schematic of SiC fiber oxidation with discretization of SiO_2 scale is in figure 1. There are two sources of stress. The first is the elastic constraint of the 2.2× volume expansion accompanying oxidation. The second is the circumferential expansion of old scale as it is radially displaced outward by formation of new scale (Fig. 1). This creates tensile hoop stress (σ_θ) in the outer scale,[16] and tensile axial stress (σ_z) by the Poisson effect.

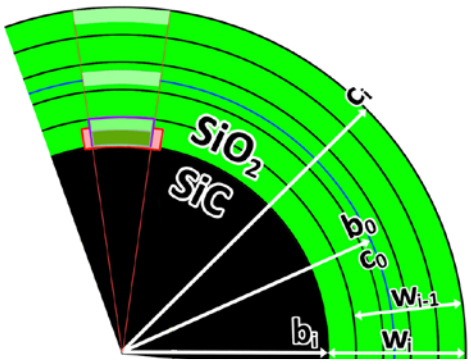

Figure 1. Schematic of SiC fiber oxidation.

The large volume expansion raises concerns for growth stress modeling. Elastic constraint of the 2.2× volume expansion causes ~25 GPa compressive stress in SiO_2, much larger than stresses for which linear elasticity is valid.[4] However, high shear stresses relax very rapidly to values appropriate for linear elasticity if SiO_2 viscosity is shear-stress dependent,[6, 17-18] and discretization can confine incremental stress differences to values appropriate for linear theory.[7, 19-20] General models of oxidation growth stress are coupled diffusion-reaction and fluid-mechanical problems.[19] The oxygen diffusion rate drives the rate that stress in the oxide is generated. Stress, in turn, affects the oxygen diffusion rates. The experimentally measured oxidation rates for SiC inherently include the effect of growth stress. The effect of stress on oxidation rate will therefore not initially be considered when modeling growth stress.

The following assumptions are used in modeling the growth stress: 1. Oxidation volume expansion is dilational. 2. Stresses resulting from constraint of oxidation expansion are relaxed by flow of SiO_2 with shear stress-dependent viscosity.3. Discretization of oxidation to small increments allows use of linear elasticity. 4. Growth stress effects on oxidation kinetics are not considered. 5. Stress relaxation in the SiC fiber is negligible.

Fiber Oxidation Kinetics

Fiber oxidation kinetics will not deviate significantly from flat-plate geometry kinetics until the oxidation product for 12 μm diameter fibers is several microns thick.[1, 9, 21] SiO_2 thickness (**w**) (Fig. 1) therefore obeys Deal-Grove kinetics for flat-plate geometry:[1-2, 22]

$$w = \frac{1}{2}A\sqrt{1+\frac{4Bt}{A^2}} - 1 \qquad (1)$$

The parabolic and linear rate constants are **B** and **B**/**A**, respectively. **B** and **A** obey the usual Arrhenius relationships. The SiC radius (**b**) after oxidation is (Fig. 1):

$$\mathbf{b} = \sqrt{w^2(\Omega^2-\Omega)+b_o^2} - \Omega w \qquad (2)$$

where $\mathbf{b_o}$ is the original fiber radius and $\boldsymbol{\Omega}$ is the SiC/SiO_2 molar volume ratio.

Elastic Growth Stress

The elastic stresses and strains are determined by modification of a method used for sequentially deposited coatings.[23] For discretized fiber oxidation, the “deposition” sequence is

reversed; the last oxide increment forms at the SiC-SiO_2 interface, and the oldest is at the surface. The system is divided into the unoxidized SiC fiber, the SiO_2 added from time **t**(i -1) to **t**(i) at the SiC-SiO_2 interface, and the outer SiO_2 increment added from **t**(0) to **t**(i-1) (Fig. 1). The axial, radial, and hoop stresses in the SiC fiber at time **t**(i) are $\sigma_z^{SiC}(i)$, $\sigma_r^{SiC}(i)$, and $\sigma_\theta^{SiC}(i)$ respectively, and in the two SiO_2 increments are $\sigma_z^{SiO2}(i)$, $\sigma_r^{SiO2}(i)$, $\sigma_\theta^{SiO2}(i)$ and $\sigma_z^{SiO2}(i\text{-}1)$, $\sigma_r^{SiO2}(i\text{-}1)$, $\sigma_\theta^{SiO2}(i\text{-}1)$, respectively. The effect of the i^{th} SiO_2 increment on elastic growth stresses is found using strain compatibility equations, which is outlined in detail in other publications.[15] Stresses in older increments are updated with the stress values calculated for the most recent increment.

Relaxation of Elastic Stress

The relaxation of the elastic stresses for all increments (j=1 to i) in time increment $\Delta t = t(i) - t(i\text{-}1)$ are calculated next. Shear stress relaxation obeys a Maxwell viscoelastic model,[6, 24] and the Eyring model for shear-stress (τ) dependence of glass viscosity (η) is used for SiO_2.[6, 10, 24-26] The initial elastic shear stress at **t**(i -1) is τ_o. The relaxation of τ_o to a new value (τ) in time increment Δt is:

$$\tau = \frac{4kT}{V_c}\,\mathrm{Coth}^{-1}\left[\frac{e^{\frac{Gt}{\eta_o}}}{\sqrt{\mathrm{Tanh}\left[\frac{V_c\tau_o(j)}{4kT}\right]^2}}\right] = 2\tau_c\,\mathrm{Coth}^{-1}\left[\frac{e^{\frac{Gt}{\eta_o}}}{\sqrt{\mathrm{Tanh}\left[\frac{\tau_o(j)}{2\tau_c}\right]^2}}\right] \qquad (3)$$

where **G** is the SiO_2 shear modulus, V_c is the activation volume for plasticity in SiO_2. **k** is Boltzmann's constant, τ_c is the critical shear stress above which plasticity is significant (typically ~100 MPa), and η_o is the stress-free SiO_2 viscosity that has an Arrhenius temperature dependence.[27] τ_o is determined from the principal stresses for all the increments (j=1 to i) by the usual methods.[28]

Relaxation of $\sigma_\theta(j)$and $\sigma_z(j)$ is proportional to $\tau(j)/\tau_o(j)$ and to their difference with $\sigma_r(j)$, which is a boundary condition, being zero at the SiO_2 surface and near zero elsewhere. The relaxed values of $\sigma_\theta(j)$and $\sigma_z(j)$ ($\sigma_\theta(j)'$ and $\sigma_z(j)'$) are determined by solution of:

$$\begin{bmatrix}\sigma_\theta(j)' & 0\\ 0 & \sigma_z(j)'\end{bmatrix} = \frac{\tau(j)}{\tau_o(j)}\begin{bmatrix}\sigma_\theta(j)-\sigma_r(j) & 0\\ 0 & \sigma_z(j)-\sigma_r(j)\end{bmatrix} + \begin{bmatrix}\sigma_r(j) & 0\\ 0 & \sigma_r(j)\end{bmatrix} \qquad (4)$$

Radial Displacement and Hoop Stress Generation

Relaxation expands the SiO_2 scale radially. The individual radial displacement of the j^{th} increment (u_r) is:

$$u_r(j) = \frac{\Omega_{SiO_2}}{\Omega_{SiC}\left(1+\varepsilon_z^{SiO2}(j)+\varepsilon_\theta^{SiO2}(j)+\varepsilon_z^{SiO2}(j)\varepsilon_\theta^{SiO2}(j)\right)} - 1 \qquad (5)$$

where strains in [5] are calculated from the stresses in [4]. The total radial displacement of the j^{th} increment is the sum of the displacements of younger increments. This adds hoop strain ($\varepsilon_\theta^{SiO2}$) to outer layers as they are forced to a larger circumference (Fig. 1). The new hoop strain in each increment is:

$$\varepsilon_{\theta}^{SiO2}(j)' = \varepsilon_{\theta}^{SiO2}(j) + \sum_{j}^{i} u_r(j)\frac{b(j-1)-b(j)}{b(j)} \quad (6)$$

Recalculation of Elastic Stress in the Scale and SiC Fiber after Radial Displacement

The stresses in each SiO_2 increment are recalculated for $\boldsymbol{\varepsilon_{\theta}}^{SiO2}(j)'$ by solving the three strain compatibility equations for the three principal stresses. Revised axial stress $\boldsymbol{\sigma_z}^{SiC}$ is computed from the force exerted by the SiO_2 scale, which is the sum of the axial stress in each SiO_2 increment × area of that increment:

$$\sigma_z^{SiC}(i) = -\sum_{j=1}^{i-1} \frac{\sigma_z^{SiO2}(j)[2c(i)(w(j)-w(j-1)+w(j)^2-w(j+1)^2]}{b(i)^2} \quad (7)$$

where **c** is the scale + fiber radius. The revised radial and hoop stress in the SiC fiber are calculated by determining the net pressure ($\mathbf{p_n}$) from the sum of the pressures in each annular increment:

$$\sigma_r^{SiC}(i) = \sigma_{\theta}^{SiC}(i) = -p_n = -\sum_{j=1}^{i-1} \sigma_{\theta}^{SiO2}(j)\frac{w(j)-w(j-1)}{b(i)} \quad (8)$$

These revised stresses are added to the next increment i as the program loops back to equations [1 -8]. For SiC oxidation when **w(i)** << **b(i)**, the stress in SiC is much smaller than that in SiO_2.

RESULTS AND DISCUSSION

Growth stress calculations were done using [1-8] using scale discretization to 500 layers (i=500). Calculations were done for oxidation of SiC fiber for amorphous scales of 500 nm thickness (**w**) at 700, 800, 900, 1000, 1100, 1200, and 1300°C (Fig. 2). The sensitivity of these

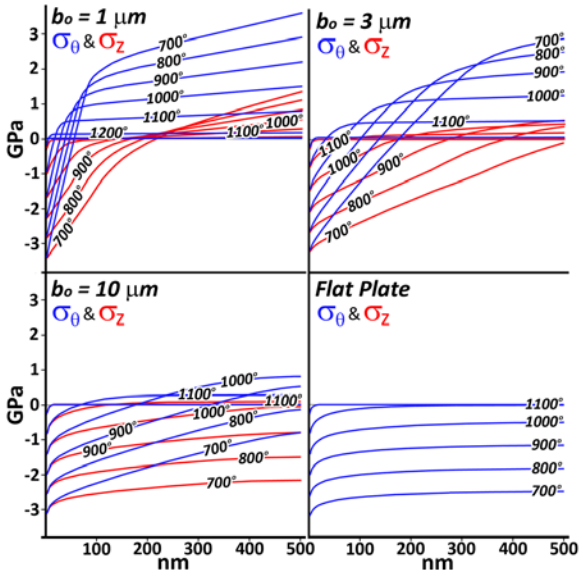

Figure 2. Calculations of hoop stress ($\boldsymbol{\sigma_{\theta}}$ - blue) and axial stress ($\boldsymbol{\sigma_z}$- red) throughout a 500 nm thick SiO_2 scale on 1, 3, and 10 μm radii SiC fibers, and SiC flat plates.

calculations to 10× changes in scale viscosity (η_o) and oxidation kinetics parameters ($\mathbf{B_o}$) are shown in figure 3. The Deal-Grove oxidation kinetics for SiC fiber have been reported for dry air between 700 and 1300°C, with $\mathbf{A_o}$ = 6.5 × 10^{-4} m, $\mathbf{B_o}$ = 1.2 × 10^{-8} m^2/s, $\mathbf{Q_A}$ = 111 kJ/mol, and $\mathbf{Q_B}$ = 249 kJ/mol.[1-2] A full list of all parameters used in the calculations is published.[15] The variation in growth stress with change in fiber radius was examined by calculations using $\mathbf{b_o}$ = 1 μm, 3 μm, 10 μm and "flat-plate" $\mathbf{b_o}$ →∞ (1 km). Calculations for other thicknesses and for crystallized scales are reported elsewhere.[15]

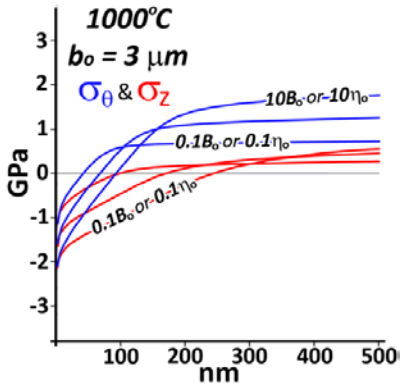

Figure 3. Change in σ_θ and σ_z growth stresses with change in viscosity (η_o) or parabolic oxidation kinetics ($\mathbf{B_o}$) parameters.

The changes of σ_θ and σ_z throughout the scale with change in $\mathbf{b_o}$ at 700°C to 1300°C are evident (Fig. 2). As fiber radius ($\mathbf{b_o}$) increases, σ_θ and σ_z become less tensile and more compressive. σ_z is driven towards tensile values by the Poisson effect from tensile σ_θ caused by outward radial expansion. For a 1 μm radius fiber, tensile σ_θ develops at the scale surface at all temperatures, and is >3 GPa at 700°C; tensile σ_z is > 1 GPa. For a 10 μm radius fiber, tensile σ_θ does not develop until $\mathbf{T}$ > 850°C and reaches a maximum of about 600 MPa at 1000°C; tensile σ_z does not develop until ~1100°C and reaches 100 MPa at that temperature. Compressive elastic stress of ~-25 GPa for σ_θ and σ_z is rapidly relaxed to ~-4 GPa at 700°C and ~-1 GPa at 1200°C just 1 nm away from the SiC-SiO_2 interface. At T >1200°C SiO_2 viscosities are so low that stress levels are insignificant at scale locations more than 20 nm from the SiC-SiO_2 interface. For flat plates $\sigma_\theta = \sigma_z$, and stress is always compressive. Note that a 500 nm scale takes ~10^8 s to form at 700°C and ~10^5 s to form at 1000°C, so the latter is of more practical interest. Calculations for crystalline SiO_2 scale and for several other scale thicknesses are reported elsewhere.[15] Crystalline scale viscosities are much higher than amorphous scale viscosities, so growth stresses are also larger. The carbon introduced in SiO_2 scales during SiC oxidation causes uncertainty in the actual SiO_2 viscosity (η_o).[15] Effects of a 10× increase or decrease in η_o and $\mathbf{B_o}$ on growth stress at 1000°C for $\mathbf{b_o}$ = 3 μm are shown in figure 3. A 2× difference in σ_θ is evident. Differences between the effects of η_o and $\mathbf{B_o}$ on growth stress are only significant for very thin scales.

For the 500 nm thick scale a "continuous-state" develops for σ_θ tensile stress for T > 900°C for $\mathbf{b_o}$ = 3 μm and T > 1000°C for $\mathbf{b_o}$ = 10 μm. For thicker scales the continuous-state region develops at lower temperatures. For $\tau < \tau_c$ of 100 MPa [16] where a stress–free viscosity (η_o) [17] is applicable, an analytical expression for the continuous-state hoop stress [σ_θ(ss)] can be derived:[15]

$$\sigma_\theta\,(ss) = \frac{2B\left(\frac{1}{\Omega} - 1\right)\eta_o}{wb} \qquad (9)$$

For τ > 100 MPa the stress dependence of viscosity is significant, and the shear stress-dependent viscosity η must be substituted for η_o.[15]

SUMMARY AND CONCLUSIONS

A method to calculate the all growth stress components in SiO_2 scales generated by the 2.2× volume expansion during SiC fiber oxidation was developed. The method can be applied to fibers of other materials. High compressive hoop and axial stresses of ~25 GPa are very quickly relaxed at all temperatures. Radial expansion creates tensile hoop stress in the outer scale. Tensile hoop stress eventually drives axial stress to a tensile state by the Poisson effect. Tensile hoop and axial stress can reach values > 3 and 1 GPa, respectively for oxidation for long times at 700° - 900°C on 1 μm radius SiC fibers. At temperatures greater than 1200°C growth stresses are quickly relaxed to negligible levels by viscous flow of SiO_2. The accuracy of the growth stress calculation is likely to be limited by the accuracy of the amorphous silica viscosity. Tensile hoop stresses reach steady-state values that can be described by analytical expressions.

REFERENCES

1. R.S. Hay, G.E. Fair, R. Bouffioux, E. Urban, J. Morrow, A. Hart, M. Wilson, Ceram. Eng. Sci. Proc. , 32 (2011) 39-54.
2. R.S. Hay, G.E. Fair, R. Bouffioux, E. Urban, J. Morrow, J. Somerson, A. Hart, M. Wilson, J. Am. Ceram. Soc., 94 (2011) 3983-3991.
3. G. Chollon, R. Pallier, R. Naslain, F. Laanani, M. Monthioux, P. Olry, J. Mater. Sci., 32 (1997) 327-347.
4. K. Garikipati, V.S. Rao, J. Computational Physics, 174 (2001) 138-170.
5. V.S. Rao, T.J.R. Hughes, Int. J. Numerical Methods in Engineering, 47 (2000) 341-358.
6. P. Sutardja, W.G. Oldham, Electron Devices, IEEE Transactions on, 36 (1989) 2415-2421.
7. A. Pomp, S. Zelenka, N. Strecker, W. Fichtner, IEEE Trans. Elec. Dev., 47 (2000) 1999-2007.
8. M. Uematsu, H. Kageshima, K. Shiraishi, M. Nagase, S. Horiguchi, Y. Takahashi, Solid-State Electronics, 48 (2004) 1073-1078.
9. D.-B. Kao, J.P. McVittie, W.D. Nix, K.C. Saraswat, IEEE Trans. Electron. Dev., 35 (1988) 25-37.
10. C.S. Rafferty, L. Borucki, R.W. Dutton, Appl. Phys. Lett., 54 (1989) 1516-1518.
11. E. Oh, J. Walton, D. Lagoudas, J. Slattery, Acta Mechanica, 181 (2006) 231-255.
12. A. Mihalyi, R.J. Jaccodine, T.J. Delph, Appl. Phys. Lett., 74 (1999) 1981-1983.
13. J.-Y. Yen, J.-G. Hwu, J. Appl. Phys., 89 (2001) 3027-3032.
14. W. Gauthier, F. Pailler, J. Lamon, R. Pailler, J. Am. Ceram. Soc., 92 (2009) 2067-2073.
15. R.S. Hay, J. Appl. Phys., 111 (2012) 063527.
16. C.H. Hsueh, A.G. Evans, J. Appl. Phys., 54 (1983) 6672-6686.
17. M. Navi, S.T. Dunham, J. Electrochem. Soc., 144 (1997) 367-371.
18. S.M. Hu, J. Appl. Phys., 70 (1991) R53-R80.
19. P. Causin, M. Restelli, R. Sacco, Computer Methods in Applied Mechanics and Engineering, 193 (2004) 3687-3710.
20. V. Senez, D. Collard, P. Ferreira, B. Baccus, IEEE Trans. Elec. Dev., 43 (1996) 720-731.
21. L.O. Wilson, R.B. Marcus, J. Electrochem. Soc., 134 (1987) 481-490.
22. B.E. Deal, A.S. Grove, J. Appl. Phys., 36 (1965) 3770-3778.
23. Y.C. Tsui, T.W. Clyne, Thin Solid Films, 306 (1997) 34-51.
24. V. Senez, D. Collard, B. Baccus, M. Brault, J. Lebailley, J. Appl. Phys., 76 (1994) 3285-3295.
25. H. Eyring, J. Chem. Phys., 4 (1936) 283-291.
26. T. Uchida, K. Nishi, Jap. J. Appl. Phys., 40 (2001) 6711-6719.
27. R.H. Doremus, J. Appl. Phys., 92 (2002) 7619-7629.
28. H.J. Frost, M.F. Ashby, Deformation Mechanism Maps, Pergamon Press, 1982.